Characterization of Radiophotoluminescence Dosimeters Under X-Ray Irradiation at High Doses

M. Ferrari, Y. Q. Aguiar, *Member, IEEE*, A. Hasan, A. K. Alem, R. García Alía, *Member, IEEE*, A. Donzella, D. Pagano, L. Sostero, A. Zenoni, and S. Girard, *Senior Member, IEEE*

***Abstract*— A characterization of radiophotoluminescence (RPL) dosimeters at high doses of X-ray radiation for applications in high-radiation areas is presented. Commercial FD-7 silver-doped phosphate glasses (1.5 × 8.5 mm) in use at CERN for passive dosimetry are irradiated using commercial X-ray tubes. A 1.5-mm-thick aluminum filter is used to harden the X-ray spectrum and improve dose homogeneity. Two irradiation campaigns are presented, targeting doses ranging from about 1.3 kGy to 0.46 MGy and dose rates from about 0.6 to 6.3 kGy/h, respectively. Monte Carlo (MC) simulations performed with PHITS allowed the determination of a factor to convert the dose to water, into the average absorbed dose to RPL material. The found conversion factor is validated by the achieved measurements. The results evidence a satisfactory agreement between the absorbed doses delivered with X-rays and the readout results, based on Co-60 gamma calibration.**

***Index Terms*— High-radiation areas, Monte Carlo (MC) simulations, radiation monitoring, radiophotoluminescence (RPL) dosimeter, X-rays.**

I. Introduction

THE accelerator complex at CERN produces intense mixed radiation fields, which pose a risk of damaging materials and electronic components situated within its tunnels and alcoves [1], [2]. To ensure the safety of personnel and equipment of the accelerator complex, it is crucial to employ reliable dosimetry systems. At CERN, different passive dosimeters are placed in selected positions to measure the total dose absorbed during operation by specific radiation-sensitive equipment [3]. Radiophotoluminescence (RPL) dosimeters are considered promising for having unique features including small size, linear response with accumulated dose up to tens of Gy, low dependency on energy, reproducible response, nondestructive multiple readout capability, and long stability against fading effects [4], [5], [6], [7], [8], [9], [10], [11].

RPL dosimeters can accordingly find application as passive dose monitors in a wide range of radiation environments, such as particle accelerators, high-power targets, fission and fusion technologies, medical physics, space exploration, and the field of radioactive waste management. They are routinely used at CERN in a wide range of areas and conditions, supporting several irradiation activities, such as the ones related to the radiation to electronics project [2], [12], [13], [14]. For example, RPL dosimetry service is often involved in the organization of irradiation campaigns outsourced to various external facilities for the characterization and qualification of materials and components for use in high-radiation areas, targeting doses in the MGy range [2]. RPL dosimeters are attached to the samples of interest, to gather information complementary to the standard dose assessment routinely performed by the facility staff.

At CERN, the RPL dosimeters are typically exposed to mixed radiation fields and can absorb doses up to several MGy over service time [11], [15], and these levels exceeding their typical use [8], [9], [10]. Therefore, a custom readout system has been developed at CERN to extend the use of RPL dosimeters for doses up to the MGy range [11], [16].

RPL readout systems require adjustments and different calibrations depending on the specific radiation environment for a correct estimate of the total absorbed dose [8]. In this regard, characterization and calibration of RPL dosimeters in different radiation conditions and the correlation between them are essential for a complete understanding of their response, especially at high doses and in mixed-field radiation environments. In these conditions, the available data are limited in comparison to more standard gamma radiation, traditionally used for calibration. Dependence on irradiation conditions such as temperature, dose rate, radiation energy spectrum, and other irradiation parameters possibly relevant for their application need to be assessed as well [9].

Manuscript received 18 December 2023; revised 5 February 2024; accepted 8 February 2024. Date of publication 12 February 2024; date of current version 16 August 2024. The work of L. Sostero was supported by the European Union (Piano Nazionale di Ripresa e Resilienza – Next Generation EU – Decreto Ministeriale 352/2022). *(Corresponding author: M. Ferrari.)*

M. Ferrari, A. Hasan, and A. K. Alem are with CNRS, Institut d'Optique Graduate School, Laboratoire Hubert Curien UMR 5516, Université Jean Monnet Saint-Etienne, 42023 Saint-Etienne, France (e-mail: matteo.ferrari@univ-st-etienne.fr).

Y. Q. Aguiar and R. García Alía are with CERN, 1211 Geneva, Switzerland (e-mail: ygor.aguiar@cern.ch).

A. Donzella, D. Pagano, L. Sostero, and A. Zenoni are with Dipartimento di Ingegneria Meccanica e Industriale, Università degli Studi di Brescia, 25123 Brescia, Italy.

S. Girard is with CNRS, Institut d'Optique Graduate School, Laboratoire Hubert Curien UMR 5516, Université Jean Monnet Saint-Etienne, 42023 Saint-Etienne, France, and also with Institut Universitaire de France (IUF), Ministère de l'Enseignement Supérieur et de la Recherche, 75005 Paris, France.

Color versions of one or more figures in this article are available at https://doi.org/10.1109/TNS.2024.3365272.

Digital Object Identifier 10.1109/TNS.2024.3365272

Additionally, there is a general interest in exploring alternatives to standard gamma sources, such as accelerator-driven X-ray tubes and electron beams, to irradiate various types of samples. These irradiation activities serve a large variety of applications, satisfying the needs of the market, mostly focused on sterilization activities, and scientific and technological applications [17]. In fact, it remains to be fully clarified whether equal absorbed doses delivered using different radiation types and in different irradiation conditions induce equal effects. This needs to be further investigated, especially at very high doses, where data are mostly lacking [18].

This work presents a new experimental characterization study on the RPL response under high X-ray doses, ranging between 1 kGy and about 0.5 MGy. A dedicated irradiation setup realized using an aluminum (Al) filter is proposed to ensure better dose homogeneity in the dosimeter volume while maintaining a sufficiently high dose rate. Samples are irradiated using a commercial X-ray source operating at 100 kV, in standard conditions. Complementary Monte Carlo (MC) simulations were carried out to support the experiments.

This article is organized as follows. First, in Section II, the fundamental mechanisms behind the RPL dosimetry are presented. In Section III, the testing methodology using a commercial X-ray source is detailed, as well as the measurement of the dose rate in the irradiation position and irradiation plan. MC simulations performed with the code PHITS are discussed in Section IV. Finally, Sections V and VI provide the discussion of the results and the conclusions, respectively.

II. RPL Dosimeters

The analyzed dosimeters are phosphate glasses doped with silver (Ag) impurities, as this element is known to be a good activator ion for RPL [4], [5]. Ionizing radiation creates electron–hole pairs in the RPL material, which are subsequently trapped at the extrinsic point defects introduced by the silver ions within the glass. The process leads to the formation of two main types of defect centers, known as RPL centers and color centers. RPL centers are responsible for the photoluminescence property of the irradiated dosimeter, referred to as the RPL signal, and color centers are responsible for the glass darkening, and corresponding light attenuation. The overall response of the dosimeter, which leads to dose determination, depends on the concentration of those centers. These dosimeters are well known for having stable centers at room temperature, with a fading effect lower than 5% per year, and low dose rate dependence [9], [10], [11].

Three different readout areas are identified, based on the evolution of the RPL response with dose [11], [16].

At relatively low doses, typically below 100 Gy, the intensity of the RPL signal is linearly dependent on the absorbed dose, while the production of color centers is generally negligible, and the dosimeter remains approximately transparent. In this range, the RPL signal alone is used for dose determination, and this represents the most common application of RPL dosimeters [8].

At intermediate dose levels, ranging between approximately 300 Gy and 6 kGy, the RPL signal saturates due to the progressively higher self-absorption caused by glass darkening. In this region, referred to as the mid-dose range, there is almost no dependency on the RPL signal on the absorbed dose, and this leads to ambiguities, making the dose readout performed using RPL light alone unreliable. The exact extension of this range depends on the irradiation conditions [11], [16], [19].

At doses higher than 6 kGy and ranging at least up to the MGy, the RPL signal progressively decreases due to the increasing self-absorption induced by glass darkening. Since the RPL signal decreases progressively in this range, the absorbed dose can be determined by its measurement alone [11].

Based on these phenomena, a custom system was developed by CERN in the frame of previous works to extend the readout of this model of RPL dosimeters to mid- and high-range doses. The system relies on a two-light measurement approach: both the RPL light and the transmittance at the selected wavelength of 445 nm, which is correlated to the formation of color centers, are measured [16]. The combined information allows the ambiguities to be solved and provides a reliable measurement technique up to high doses, as the ones present at CERN. The detailed description of this system and the calibration procedure are available in [11] and [16].

The RPL dosimeters in use at CERN, and studied in this work, are commercial GD-301 dosimeters (AGC TECHNO GLASS Company Ltd.), supplied by Chiyoda Technol, Japan [20]. These dosimeters consist of a cylindrical FD7 glass element, with a diameter of 1.5 mm and a length of 8.5 mm, which is placed in a plastic holder with a diameter of 2.8 mm and a length of 9.5 mm. They are originally designed for use in medical applications, in the field of diagnostic radiology and radiotherapy. In the context of the present work, which targets extremely high-dose applications, the dose levels generally relevant for medical applications are referred to as "low doses." Accordingly, their use is recommended by the producer in X-ray or gamma radiation fields up to a maximum dose of 10 Gy, extendable to 500 Gy, declared as reference level. In the described experiments, the FD7 glass rods have been irradiated alone, without the plastic holder. In the article, the irradiated glass rods are simply referred to as RPL samples. All the RPL dosimeters irradiated in this study are pristine, meaning that they have never been exposed to radiation before.

In a previous study, the response of these dosimeters was characterized up to the MGy dose range after irradiation in the Co-60 gamma field at the Risø HDRL Facility, Denmark [11], [21]. Dosimeter readout was performed 26 days after irradiation. CERN's readout system was calibrated based on these measurements.

III. Methodology

A. Irradiation Conditions and Setup

Irradiations were performed using the MOPERIX X-ray facility available at Laboratoire Hubert Curien (University Jean Monnet). For all the discussed irradiations, the X-ray tube operated at 100-kV voltage, and the maximum available current in these conditions corresponds to 45 mA. The used source is a commercial X-ray tube with a tungsten anode and includes a 4-mm beryllium window as a first filter [22], [23].

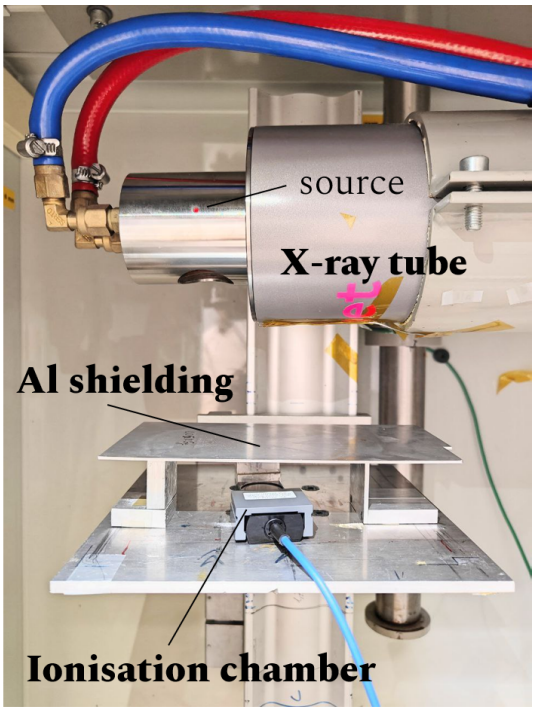

(a)

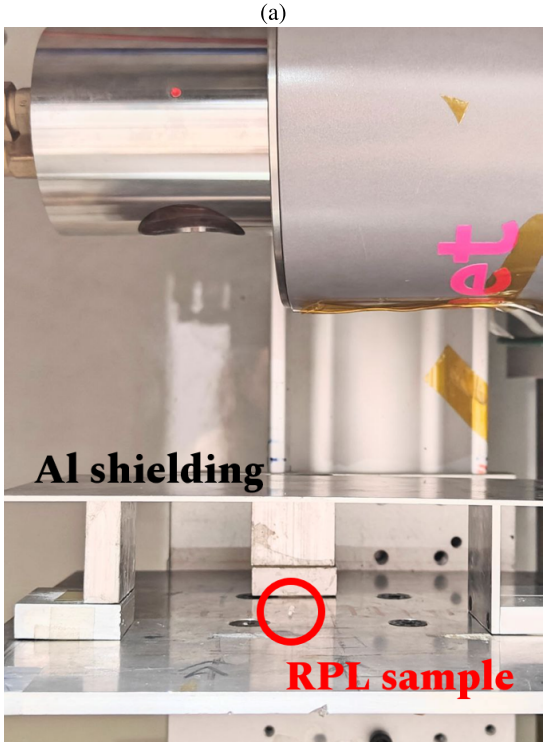

(b)

Fig. 1. Irradiation setup used for the irradiation of the dosimeters in the X-ray irradiator. (a) Dose rate measurement in the irradiation position with the ionization chamber. (b) Sample irradiation: the position of the small RPL sample is evidenced by the red circle.

The irradiation setup developed for the irradiation of the dosimeters is shown in Fig. 1. To improve dose homogeneity, as further discussed in Section IV, a 1.5-mm-thick aluminum filter was placed between the source and the sample, at about 3 cm distance from the sample surface. The X-ray tube is visible in the upper part of Fig. 1(a): the red dot corresponds to the emission point of the photons generated by the X-ray tube; the beryllium window is positioned below it, defining an emission cone for the photons.

During irradiation, the RPL samples are positioned horizontally, so that the X-ray beam impinges perpendicularly to the cylinder axis. The distance between the sample and the source was around 8 cm.

Filtration is a widely used technique to achieve desired radiation qualities. The use of standard setups for X-ray beam filtering is recommended, to meet the precision requirements of diagnostic radiology applications and for the calibration of dosimetric equipment for radiology [24]. In the present work, the used setup is functional for the irradiation of 1.5-mm-thick FD-7 glass samples with satisfactory homogeneity in an X-ray facility normally used for the irradiation of optical fiber samples in unfiltered conditions. This nonstandard setup is adjustable and easy to assemble and remove, making it compatible with the dynamic operation of the facility, which serves multiple users, and in which permanent modifications of the configuration of the irradiation chamber are not possible. Future works will aim at establishing and developing a standardized irradiation setup compatible with the facility requirement and allowing the irradiation of various samples using different radiation qualities.

The dose rate at the sample position in each configuration was measured using a PTW ionization chamber 23 344, visible in Fig. 1(b) below the Al shielding. The ionization chamber has 2 cm diameter, with a sensitive volume of 0.2 cm^3. It was centered on the position occupied by the sample during irradiation.

B. Dose Rate Measurement

The chamber provides a dose rate to water at equilibrium conditions, and it is used as a reference to plan the irradiation campaigns. Considering that the dose rate was kept constant during each irradiation, the total dose to water for each irradiation can be calculated using the following equation:

$$D_w(\text{meas}) = \dot{D_W} \cdot t_{\text{irr}} \tag{1}$$

where t_{irr} corresponds to the irradiation time and $\dot{D_W}$, expressed in Gy[H_2O]/h, is the dose rate to water as measured by the ionization chamber.

An overall 10% uncertainty is associated with the estimate of $\dot{D_W}$, depending on the error on the ionization chamber readout and its resolution in comparison to the sample size. The sensitive area of the ionization chamber, is in fact, larger than the RPL sample, therefore, multiple measurements were performed by moving the position of the ionizing chamber of 1 cm in every direction to estimate the dose gradient at the sample location. A satisfactory homogeneity was found, and the dose error associated with sample positioning alone is lower than 5%. After carrying out the dose rate measurement, the sample holder position was adjusted to account for the thickness of the ionization chamber, to make sure that the RPL samples are irradiated in the position where the dose rate is measured.

TABLE I
SUMMARY OF IRRADIATION CAMPAIGNS AND OF THE CALIBRATION RESULTS

	$\dot{D_W}$ kGy[H_2O]/h	t_{irr}	$D_W(meas)$ kGy[H_2O]
D1	2.1	10 min	0.35
D2	2.1	100 min	3.5
D3	2.1	10 h	21.0
D4	2.1	60 h	125.9
DR1	1.7	108 min	3.1
DR2	0.68	270 min	3.1
DR3	0.32	9 h	3.1
DR4	0.17	18 h	3.1

C. Irradiation Plan

Two irradiation campaigns are presented, as summarized in Table I. In the first one, the dose rate was kept at a constant value for the four chosen irradiation times, which ranged from 10 min to 60 h, allowing doses ranging from the kGy to almost the MGy level to be delivered to four samples (namely, D1, D2, D3, and D4).

In the second irradiation campaign, the same target dose $D_w = 3.1$ kGy[H_2O] was delivered to four samples (namely, DR1, DR2, DR3, and DR4) using different dose rates ranging from 1.7 kGy[H_2O]/h (DR1) down to 0.17 kGy[H_2O]/h (DR4), by correspondingly increasing t_{irr} from 108 min to 18 h. The dose rate is lowered by proportionally decreasing the current value from a maximum of 45 mA to a minimum of 4.5 mA, leaving the irradiation position unaltered.

The irradiations presented in this study mostly target the high-dose range.

IV. MC SIMULATIONS

Simulations were realized by using the MC code PHITS (3.30) [25], with the following scopes. First, the dose profile as a function of the sample depth is calculated, to evaluate the dose homogeneity within the RPL sample volume, and dose attenuation due to its thickness. The aim is to verify the possibility of using the X-ray field available at the facilities, having a lower penetration in comparison to Co-60 gamma radiation, for the irradiation of a 1.5-mm-thick RPL sample. The irradiation of relatively large samples with X-ray radiation is, in fact, in many cases, challenged by the lack of dose uniformity in the volume of the sample to be irradiated [18], [26]. To improve homogeneity, the impact of a 1.5-mm Al shielding on the X-ray spectrum and on the RPL dosimetry is computed.

Photon fluence spectra are then characterized in different configurations. Additionally, the absorbed dose to two different materials, water, and the FD7 glass, composing RPL samples, is evaluated and compared. A conversion factor between the dose absorbed by water and by RPL samples in these specific irradiation conditions is determined. To these purposes, a simplified geometry including the photon source, the X-ray tube structure, the RPL sample (or the equivalent water sample),

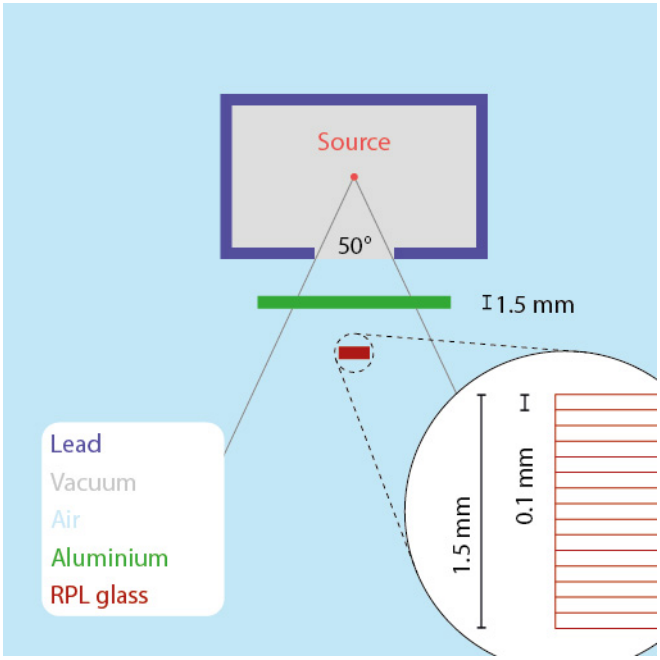

Fig. 2. Schematic representation (not in scale) of the used simulation model, in the shielded configuration. It includes the source position (red dot), the lead box (blue) filled with vacuum (gray), the Al filter (green), and the RPL sample (red), whose structure is zoomed in the circle. The air is in pale blue. In the unshielded configuration, the Al shielding is simply removed and replaced with air. For the simulations in water, the RPL glass material is replaced with water.

and the Al shielding for the filtering effect is realized in PHITS. The statistical error associated with all the simulated quantities is lower than 3%.

A. Model Description

An isotropic photon source has been generated using as input the energy spectrum provided by SpekPy v2.0, a toolkit commonly used to model X-ray tube spectra [27]. The used spectrum corresponds to the one produced by a standard X-ray irradiator with a tungsten target operating at 100 kV, with an anode angle of 30°, and already including a filtration corresponding to a 4-mm Be window. For this reason, the Be window is not included in the model. The spectrum produced by SpekPy is then generated in PHITS using an isotropic source and then transported in the realized geometry. The EGS5 model for the simulation of electrons and photons with energies higher than 1 keV is used [25].

In the used model, as schematically represented in Fig. 2, an isotropic point photon source is located in the origin of the axes. The X-ray tube structure is modeled as a lead box, with a thickness of 0.4 mm. The inner box volume is filled with a vacuum. The rest of the facility, simulated as a cube of 20 cm side, is filled with air. The emission cone of the photons is visible in Fig. 3.

Simulations are realized in two main configurations: without any additional filtration and with an additional 1.5-mm-thick Al filter placed between the source and the sample, at a 3.0 cm distance from the samples. In the article, they are referred to as unshielded and shielded configurations, respectively.

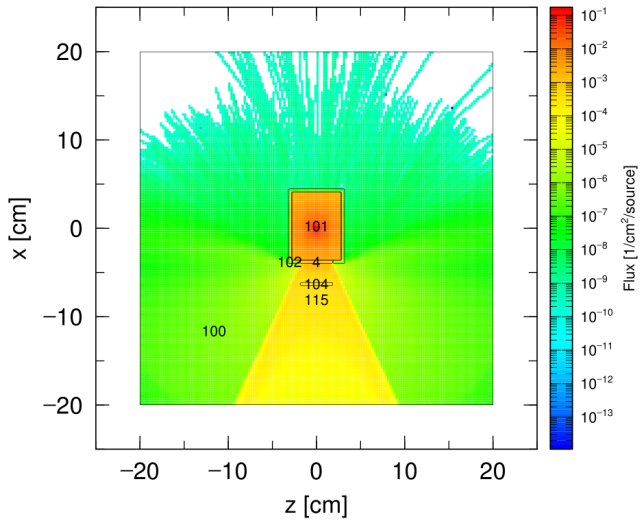

Fig. 3. Vertical section representing the tracks of the transported photons in the realized PHITS model of the irradiation facility [25]. The 50° emission cone of the radiation outside the X-ray tube box is clearly visible. The position of the shielding (label 104 in the plot) and of the sample (115) are visible.

TABLE II
MATERIAL COMPOSITION AND DENSITY OF THE FD7 GLASS ROD (GD-301) [11]

	Density [g/cm^3]	O [wt-%]	P [wt-%]	Na [wt-%]	Al [wt-%]	Ag [wt-%]
FD7	2.6041	51.16	31.55	11.0	6.12	0.17

The RPL sample is modeled as a rectangular box with dimensions 8.5 × 1.5 × 1.5 mm. Table II provides relevant information used in the simulations concerning the composition and the density of the glass material constituting the RPL dosimeters.

Simulations not reported here showed that the approximation made on the sample geometry, which is modeled as a box instead of a cylinder to better study the dose dependency as a function of the sample thickness, does not impact the average dose absorbed by the sample in irradiation position [28].

The fluences and doses here reported are expressed in cm^{-2}/primary and Gy/primary, respectively, and are intended to be used for comparative assessments only.

B. Photon Energy Spectra

Fig. 4 presents the photon fluence energy spectrum computed in a reference position in the shielded (orange) and unshielded (black) configuration. The used energy bin corresponds to 0.5 keV.

The spectrum results from two well-known main contributions, clearly visible in Fig. 4. The bremsstrahlung contribution is continuous, accounting for photons up to a maximum energy of 100 keV, depending on the tube voltage, in this case 100 kV. The bremsstrahlung component is higher at lower photon energies and progressively decreases approaching the maximum energy threshold. The superimposed intense and narrow discrete peaks correspond to the characteristic X-ray emission typical of the target material, in this case, tungsten [23], [29].

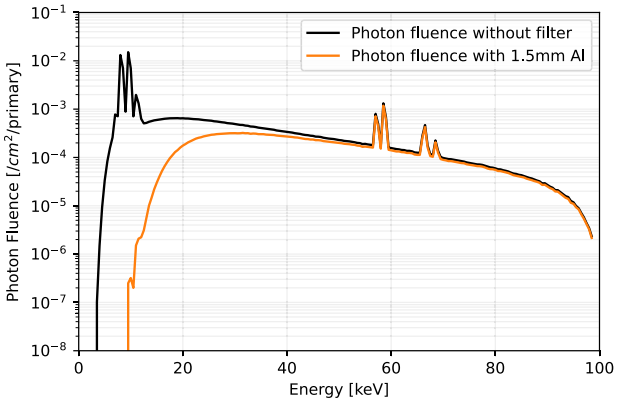

Fig. 4. Simulated impact of a 1.5-mm Al filter on the analyzed photon energy spectrum at the sample position.

The beryllium window, already incorporated in both these spectra, is responsible for the strong attenuation up to approximately 5–9 keV [27], [28]. By comparing the two spectra, it can be noted that the lower part of the energy spectrum, approximately up to 15–20 keV, is strongly attenuated by the 1.5-mm-thick Al shielding. In this context, filters are used to harden the available photon spectrum (to increase the average photon energy) by attenuating low-energy photons, which can be responsible for a highly inhomogeneous dose distribution in relatively thick samples, including the ones of interest for this study.

The half value layer (HVL), corresponding to the thickness of material to attenuate the measured quantity to one-half of its initial value, is a metric commonly used to describe the radiation quality, and in particular, it quantifies the hardness, of a given radiation spectrum [24]. Spekpy provides HVL expressed in terms of air kerma [27]. For aluminum, HVL = 0.081 mm in the unshielded case, while it raises to HVL = 2.2 mm in the shielded configuration.

C. Dosimetry in RPL and Water Samples

To evaluate the dose attenuation as a function of the sample thickness in the analyzed X-ray spectra, the absorbed dose has been simulated by dividing the sample geometry in 0.1-mm-thick slabs, as schematically represented in Fig. 2. Dose simulations have been performed in two different samples, having the same geometry: FD7 glass, used for the construction of the RPL samples, and water, simulated for reference. Doses in the FD7 material sample (D_{RPL}(sim)) and in water (D_W(sim)) are reported in Fig. 5 as a function of the sample depth. Simulations are shown in two different configurations: unshielded [Fig. 5(a)] and shielded [Fig. 5(b)].

To quantify the dose inhomogeneity in the sample, the dose uniformity ratio (DUR = $D_{\max}/D_{\min}$) has been calculated using the dose values simulated in the sample slabs. The closer the DUR is to 1, the more homogeneous the dose distribution in the sample. The DUR, often used as a simple way to compare dose homogeneity in irradiated samples, is here used to assess the overall shielding effect and to evaluate the feasibility of the irradiation experiments [18], [30].

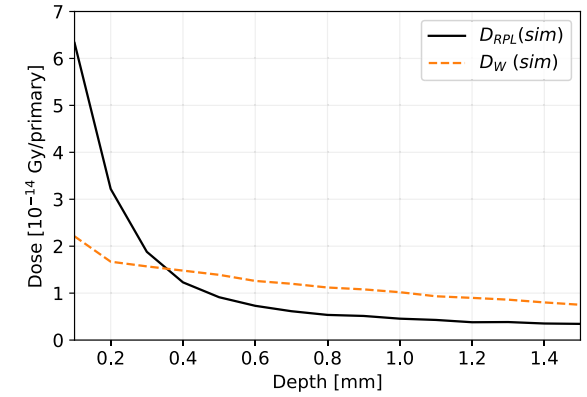

(a)

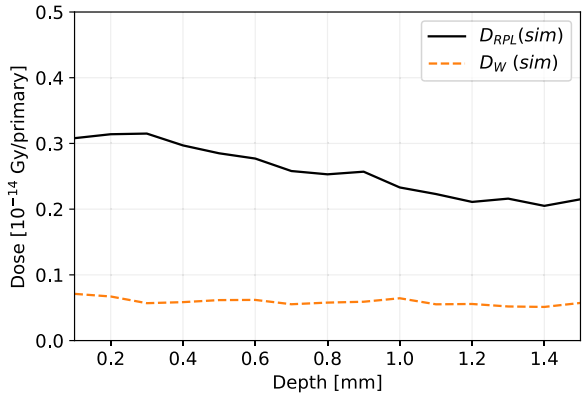

(b)

Fig. 5. Simulated absorbed dose to water (orange) and RPL material (black) as a function of the sample depth for two configurations: (a) unshielded and (b) with a 1.5-mm Al filter placed at a 3 cm distance from the sample.

In the unshielded configuration, as shown in Fig. 5(a), the DUR for the RPL sample corresponds to 18.3. This value is obviously too large to irradiate the RPL dosimeters with sufficient homogeneity. In the shielded configuration, the DUR value is highly improved, and decreases to about 1.6, as shown in Fig. 5(b). This value represents a satisfactory compromise between the desired homogeneity and the dose rate reduction due to the shielding effect. The dose inhomogeneity within the sample volume can be quantified by attributing approximately a ±25% uncertainty on the average RPL dose value [28].

Low-energy photons are responsible for dose inhomogeneity observed in the unshielded configurations, as they are strongly attenuated by the first layers of the sample, where they deliver higher doses. The realized simulations confirmed the spectrum hardening achieved with the introduction of a 1.5-mm-thick aluminum filter can greatly improve the homogeneity of the dose deposited in the sample in the available X-ray field.

D. Dose to Water and Conversion Factor Estimation

The simulations in water samples are used to simulate the readout of the ionization chamber and to compute a conversion factor between D_W(meas) and the average absorbed dose to the RPL dosimeter, referred to as D_{RPL}(calc.) by using the following formula:

$$D_{\mathrm{RPL}}(\mathrm{calc}) = D_W(\mathrm{meas}) \cdot C_{\mathrm{sim}} \tag{2}$$

where the conversion factor C_{sim} comes from simulations and is defined as

$$C_{\mathrm{sim}} = \frac{\overline{D_{\mathrm{RPL}}}(\mathrm{sim})}{D_W(\mathrm{sim})_{\mathrm{EQ}}}. \tag{3}$$

$\overline{D_{\mathrm{RPL}}}$(sim) is the simulated average dose in the RPL sample and $D_W(\mathrm{sim})_{\mathrm{EQ}}$ is the simulated dose at the equilibrium in an identical volume of water, both simulated in the shielded configuration.

Using (3), a C_{sim} value of 3.7 with 25% uncertainty is found. The value refers to the selected irradiation conditions, corresponding to the radiation spectrum in the shielded configuration showed in Fig. 4, and to the specific geometry of the RPL sample. The overall uncertainty attributed to D_{RPL}(calc), corresponding to approximately 30%, is dominated by the dose inhomogeneity across the sample volume. In Section V, the simulations are compared with the experimental readout of the dosimeters.

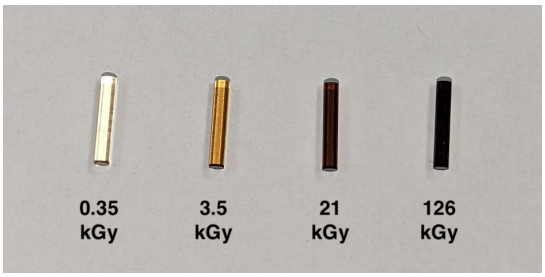

(a)

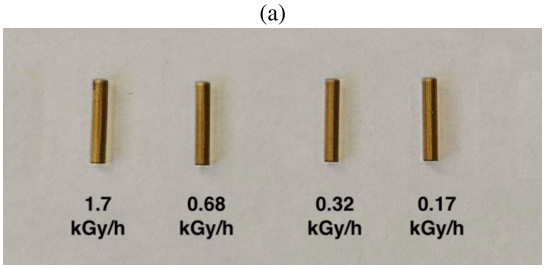

(b)

Fig. 6. Samples irradiated in the two irradiation campaigns. From left to right (a) D1, D2, D3, and D4 after irradiation and (b) DR1, DR2, DR3, and DR4 after irradiation. Absorbed dose to water and dose rate to water are indicated for reference, respectively.

V. Results and Discussion

The samples irradiated in the first and second experiment, whose irradiation conditions are summarized in Table I, are shown in Fig. 6(a) and (b), respectively.

Once the dose rate to water was measured with the ionization chamber, RPL samples were irradiated at different doses and dose rates using a dedicated sample holder (not shown in the pictures), allowing all the samples to be repeatedly placed in the same position.

As expected, a progressive glass darkening as a function of the absorbed dose is observed for the samples irradiated in the first experiment. The D1 sample is almost transparent,

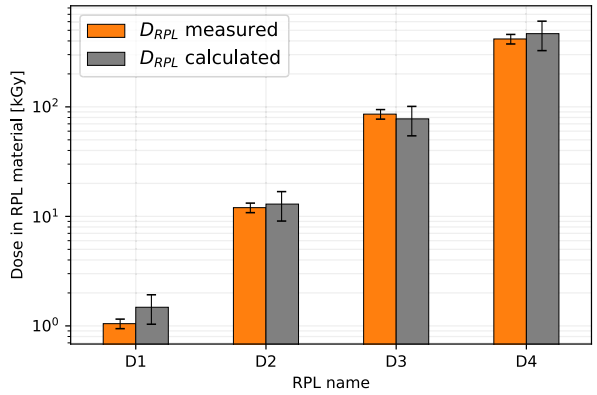

Fig. 7. Measured and calculated doses in RPL samples D1, D2, D3, and D4. The samples have been irradiated at a constant dose rate of 2.1 kGy[H_2O]/h.

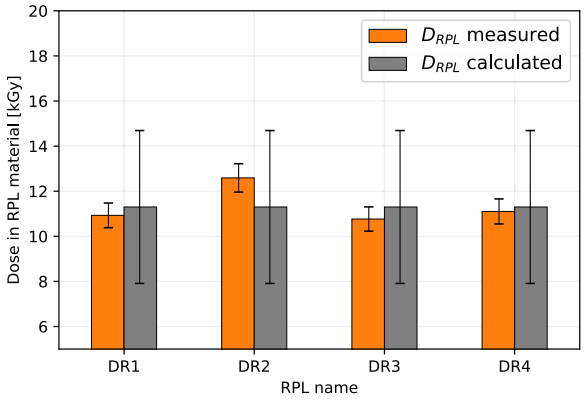

Fig. 8. Measured and calculated doses in RPL samples DR1, DR2, DR3, and DR4. Dose rates vary over one order of magnitude, as reported in Table I.

the D2 sample is yellowish, and the D3 and D4 samples are dark brown and black, respectively. By visual inspection, the radiation-induced darkening looks comparable for the DR1, DR2, DR3, and DR4 samples, as they all absorbed the same total dose.

After irradiation, a readout of all the RPL dosimeters was performed at CERN, using the system described in [11] and [16]. The standard deviation attributed to the readout system corresponds to 5%. Each dosimeter was read eight times, each time with a different spatial orientation, to ensure a correct sample positioning and alignment in the readout system. The differences between the repeated measurements are negligible in comparison to the system's uncertainty. CERN's readout system is calibrated based on a previous irradiation campaign performed in Co-60 gamma radiation [11].

Readouts were performed about 6 weeks after irradiation for D1, D2, D3, and D4 samples, and within 1 week from the end of the irradiation for DR1, DR2, DR3, and DR4 samples. In both cases, the fading effect is as a first approximation considered negligible.

The temperature at the sample position was monitored during irradiation by using thermocouples, and for all the irradiated samples it ranged between 23 °C and 27 °C.

Figs. 7 and 8 show a comparison between the dose readout D_{RPL}(meas) performed at CERN and D_{RPL}(calc) calculated as a result of the two irradiation campaigns. The doses D_{RPL}(calc) are calculated using the measured ionization chamber readout and the conversion factor achieved with the simulations as specified in (2). Both doses are expressed in Gy in FD7 material. The error bar attributed to D_{RPL}(meas) depends on the uncertainty of the readout system and corresponds to 5%. The error bar attributed to D_{RPL}(calc) is dominated by the dose inhomogeneity across the sample volume and, as discussed in Section IV, it corresponds to 30%.

The two doses are comparable within the errors, and this agreement is observed for all the irradiated samples. In particular, Fig. 7 evidences the agreement over a large dose interval, from 1 kGy to about 0.5 MGy. In Fig. 8, all the samples have been irradiated using different dose rates varied over one order of magnitude, at the same target dose. No measurable dose rate dependence is reported in the investigated range, as all the readouts are compatible with the attributed errors.

These results confirm the expected independence of the RPL signal on the dose rate and provide additional data on the dose rate effect in X-ray irradiation conditions. Agreement is found between D_{RPL}(meas) and D_{RPL}(calc), confirming the validity of used experimental procedures and of the simulated conversion factor. The coherence between the collected results confirms that by using a 1.5-mm Al shielding, dose homogeneity can be greatly improved.

The reported considerations refer to a specific dosimeter composition and geometry, and the discussed results are collected using a specific readout system tailored to this dosimeter type. The impact of the dosimeter dimension, shape, and composition on X-ray dosimetry will be considered in future studies.

VI. Conclusion

The response of RPL dosimeters with dose, delivered using a hardened X-ray spectrum, is measured over almost three decades and up to a maximum dose of approximately 0.5 MGy. The performed experiments target, in particular, the so-called high-dose range, well exceeding the ordinary applications of these dosimeters and the data usually available in the literature. A satisfactory agreement is found between the doses measured by the readout system, previously calibrated in Co-60 gamma radiation, and the calculated dose values computed by combining the ionization chamber dose rate measurements and the outcomes of MC simulations. This agreement is verified for a wide range of doses, from 1 kGy to 0.5 MGy, and a range of dose rates varying over more than one order of magnitude, from 0.17 kGy[H_2O]/h up to 2.1 kGy[H_2O]/h. Therefore, the results indicate that the standard calibration performed in Co-60 radiation in a previous work [11] remains overall valid for X-ray irradiation in the selected irradiation conditions. The found agreement also allows the computed conversion factor from the dose to water to the dose absorbed by the dosimeters in the described radiation quality to be verified.

The use of X-ray tubes allows for high doses to be delivered in reduced irradiation time, thanks to the high available dose rates. In this study, a maximum dose rate of 7.73 kGy/h in RPL material was achieved, allowing doses in the MGy range to be delivered in a few irradiation days. The problem

of dose attenuation within the sample thickness is solved by filtering the low-energy photons of the spectrum with a simple Al shielding, greatly improving the dose homogeneity in the sample volume without excessively compromising the dose rate. With this approach, the known limitations associated with the availability and accessibility of Co-60 gamma irradiation facilities for prolonged scientific activities may be overcome, as the use of alternative irradiation conditions, such as the ones produced by X-ray irradiators, is possible.

Online measurements of transmittance and radiation-induced attenuation during irradiation and its recovery after irradiation are currently being explored in the described irradiation conditions.

REFERENCES

[1] Y. Q. Aguiar et al., "Radiation to electronics impact on CERN LHC operation: Run 2 overview and HL-LHC outlook," in *Proc. 12th Int. Part. Accel. Conf.* Campinas, Brazil: JACoW, Aug. 2021, pp. 80–83.

[2] M. Ferrari et al., "'Radiation to materials' at CERN," *IEEE Trans. Nucl. Sci.*, vol. 70, no. 8, pp. 1580–1586, Aug. 2023.

[3] H. Vincke et al., "Response of alanine and radio-photo-luminescence dosemeters to mixed high-energy radiation fields," *Radiat. Protection Dosimetry*, vol. 125, nos. 1–4, pp. 340–344, Mar. 2007.

[4] K. Becker, *Solid State Dosimetry*. Cleveland, OH, USA: CRC Press, 1973.

[5] H. Schonbacher, M. Furstner, and H. Vincke, "High-level dosimetric methods," *Radiat. Protection Dosimetry*, vol. 137, nos. 1–2, pp. 83–93, Nov. 2009.

[6] D. Y. Huang and S.-M. Hsu, "Radio-photoluminescence glass dosimeter (RPLGD)," in *Advances in Cancer Therapy*, H. Gali-Muhtasib, Ed. Rijeka, Croatia: IntechOpen, 2011, ch. 25.

[7] T. Kurobori, "Performance characterisation of a real-time fiber dosimetry system using radiophotoluminescent glasses," *Jpn. J. Appl. Phys.*, vol. 57, no. 10, Sep. 2018, Art. no. 106402.

[8] T. Yamamoto, "RPL dosimetry: Principles and applications," in *Proc. AIP Conf.*, vol. 1345, May 2011, pp. 217–230.

[9] G. Okada, Y. Koguchi, T. Yanagida, S. Kasap, and H. Nanto, "Recent advances in radiophotoluminescence materials for luminescence dosimetry," *Jpn. J. Appl. Phys.*, vol. 62, no. 1, Nov. 2022, Art. no. 010609.

[10] T. Yamamoto, Y. Yanagida-Miyamoto, T. Iida, and H. Nanto, "Current status and future prospect of RPL glass dosimeter," *Radiat. Meas.*, vol. 136, Aug. 2020, Art. no. 106363.

[11] D. Pramberger, Y. Q. Aguiar, J. Trummer, and H. Vincke, "Characterization of radio-photo-luminescence (RPL) dosimeters as radiation monitors in the CERN accelerator complex," *IEEE Trans. Nucl. Sci.*, vol. 69, no. 7, pp. 1618–1624, Jul. 2022.

[12] K. Biłko et al., "CERN super proton synchrotron radiation environment and related radiation hardness assurance implications," *IEEE Trans. Nucl. Sci.*, vol. 70, no. 8, pp. 1606–1615, Aug. 2023.

[13] M. Cecchetto et al., "Electronics irradiation with neutrons at the NEAR station of the n_TOF spallation source at CERN," *IEEE Trans. Nucl. Sci.*, vol. 70, no. 8, pp. 1587–1595, Aug. 2023.

[14] G. Lerner et al., "Analysis of the radiation field generated by 200-MeV electrons on a target at the CLEAR accelerator at CERN," *IEEE Trans. Nucl. Sci.*, vol. 70, no. 8, pp. 1572–1579, Aug. 2023.

[15] M. Ferrari et al., "Design development and implementation of an irradiation station at the neutron time-of-flight facility at CERN," *Phys. Rev. Accel. Beams*, vol. 25, no. 10, Oct. 2022, Art. no. 103001.

[16] H. Vinke and J. Trummer, "Apparatus and method for determining a dose of ionizing radiation," Patent WO 1 617 32A1, Oct. 9, 2014.

[17] J. Lieberman et al., "Replacement of cobalt in medical device sterilization: Current trends, opportunities and barriers to adoption of X-ray and E-beam within the medical device sterilization market," *Arab J. Nucl. Sci. Appl.*, vol. 53, no. 4, pp. 102–111, Sep. 2020.

[18] IAEA Consultancy Meeting, "Radiation effects on polymer materials," IAEA Int. Atomic Energy Agency, Vienna, Austria, Meeting Rep. EVT1905348, Nov. 2019. [Online]. Available: http://www-naweb.iaea.org/

[19] A. Hasan, "Characterization of radio-photo-luminescence (RPL) dosimeters under high dose X-ray irradiation," M.S. thesis, EMJMD RADMEP, Univ. Jyväskylä, Katholieke Universiteit Leuven, Univ. Montpellier, Univ. Jean Monnet, Belgium, France, Saint-Etienne, France, 2023. [Online]. Available: https://jyx.jyu.fi/handle/123456789/89370

[20] Chiyoda Technol Corp. (Dec. 2021). *Dose ACE, RPL in-Vivo Dosimetry System for Medical Use, Technical Data Sheet*. Accessed: Sep. 3, 2023. [Online]. Available: https://www.c-technol.co.jp/en/

[21] A. Brynjolfsson and N. Holm, "The Co^{60} irradiation facility and the gamma field at Riso," in *Proc. Large Radiat. Sources Ind., Conf.* Warsaw, Poland: International Atomic Energy Agency, 1960, pp. 117–120. [Online]. Available: https://inis.iaea.org/

[22] (Jul. 2023). *MXR 165, X-Ray Tubes, Comet AG, Technical Data Sheet Doc. No. 50005441*. Accessed: Sep. 3, 2023. [Online]. Available: https://xray.comet.tech/

[23] A. Meyer, D. Lambert, A. Morana, P. Paillet, A. Boukenter, and S. Girard, "Simulation and optimization of optical fiber irradiation with X-rays at different energies," *Radiation*, vol. 3, no. 1, pp. 58–74, Mar. 2023.

[24] F. Pernička and I. D. McLean, "Dosimetry in diagnostic radiology: An international code of practice," Division Hum. Health, IAEA Int. Atomic Energy Agency, Vienna, Austria, Tech. Rep. 457, 2007. [Online]. Available: https://www.iaea.org/publications/

[25] T. Sato et al., "Features of particle and heavy ion transport code system (PHITS) version 3.02," *J. Nucl. Sci. Technol.*, vol. 55, no. 6, pp. 684–690, Jun. 2018.

[26] K. H. Chadwick and W. F. Oosterheert, "Dosimetry concepts and measurements in food irradiation processing," *Int. J. Radiat. Appl. Instrum. A, Appl. Radiat. Isot.*, vol. 37, no. 1, pp. 47–52, Jan. 1986.

[27] G. Poludniowski, A. Omar, R. Bujila, and P. Andreo, "Technical Note: SpekPy v2.0—A software toolkit for modeling X-ray tube spectra," *Med. Phys.*, vol. 48, no. 7, pp. 3630–3637, 2021.

[28] A. K. Alem, "Dosimetry study in an X-ray irradiator: Monte Carlo simulations and experimental results on radio-photoluminescence samples," M.S. thesis, EMJMD RADMEP, Univ. Jyväskylä, Katholieke Universiteit Leuven, Univ. Montpellier, Univ. Jean Monnet, Belgium, France, Saint-Etienne, France, 2023. [Online]. Available: https://jyx.jyu.fi/handle/123456789/89326

[29] F. H. Attix, *Introduction to Radiological Physics and Radiation Dosimetry*. Weinheim, Germany: Wiley, 1986.

[30] F. Stichelbaut et al., "The Palletron^{TM}: A high-dose uniformity pallet irradiator with X-rays," *Radiat. Phys. Chem.*, vol. 71, nos. 1–2, pp. 289–293, 2004.